Results in Engineering 32 (2026) 112141

Contents lists available at ScienceDirect

Results in Engineering

journal homepage: www.sciencedirect.com/journal/results-in-engineering

Flood-Induced Shear Failure and Floating Performance of UHPC Box Girder Bridge Using Integrated CFD-FEM Analysis

Aso Abdulghafur Faqe Rahim [a,b,*], Raizal Saifulnaz Muhammad Rashid [a,*], Nor Azizi [a], Badronnisa Yusuf [a], Adeb Qaid Al Ameri [c,*], Voo Yen lei [a], Hassan Amer Algaifi [d]

[a] Department of Civil Engineering, Faculty of Engineering, Universiti Putra Malaysia, Serdang 43400, Selangor, Malaysia
[b] Department of Water Resources, College of Engineering, University of Sulaimani, Sulaymaniyah 46001, Iraq
[c] Department of Architectural Engineering, Kingdom University, Riffa, Kingdom of Bahrain, Bahrain
[d] Institute of Energy Infrastructure, Universiti Tenaga Nasional, Jalan IKRAM-UNITEN, 43000, Kajang, Selangor, Malaysia

ARTICLE INFO

Keywords:
floating bridge
shear stress
flood-induced shear failure
computational fluid dynamics
finite element method
ultra-high-performance concrete

ABSTRACT

The vulnerability of bridges to flooding and debris impact has become a critical global concern, further intensified by climate change. This study investigates the flood-induced shear response of an ultra-high-performance concrete (UHPC) box-girder bridge without shear reinforcement, designed to temporarily float during extreme flooding and thereby enhance structural resilience and public safety. A sequential methodology was adopted using a 1:7.5 scaled UHPC box-girder bridge model, combining laboratory experiments and integrated CFD–FEM simulations to evaluate shear failure mechanisms under flood flow and debris impact. Laboratory experiments first assessed the bridge's floating capacity and shear resistance under three loading scenarios—flow-only, debris-only, and combined flow–debris loading—at velocities ranging from 0.5 to 1.0 m/s. Complementary numerical analyses were then performed using computational fluid dynamics in ANSYS to predict hydrodynamic drag forces over a wider velocity range (0.5–16 m/s), which were subsequently transferred into a finite element framework to evaluate shear stress evolution. The results demonstrate that the bridge successfully transitioned into a floating state with only 120 mm of partial submersion from its total depth of 286 mm. Under flow-only conditions, shear stresses remained below the shear capacity of 10.6 MPa even at velocities up to 15.5 m/s. In contrast, debris impact significantly amplified hydrodynamic forces, reducing the critical velocity threshold to 3.5 m/s. Based on the shear failure index, critical velocities of 16 m/s, 7 m/s, and 3.5 m/s were identified for flow-only, debris-only, and combined loading conditions, respectively. These findings highlight debris as the dominant factor governing shear vulnerability and confirm the feasibility of the proposed semi-floating UHPC bridge as a sustainable, flood-resilient alternative to conventional bridge systems.

1. Introduction

In recent years, the civil engineering community has devoted significant attention to the vulnerability of bridges under flood events. This concern arises from the increasing influence of climate change, which has amplified the frequency and intensity of sudden and unpredictable floods [1,2]. According to Arora et al. [3], floods are among the most destructive natural hazards affecting infrastructure and often impact large populations. Over the past three decades, numerous bridges worldwide have experienced partial or total failure due to flooding [4]. Such failures are commonly associated with extreme flood events in which elevated water levels submerge bridge superstructures, generating significant hydrodynamic forces and undesirable shear effects [5,6]. These structural damages result in substantial economic losses and severely hinder disaster response and recovery efforts [7]. Recent numerical studies have shown that flood-induced hydrodynamic forces can cause significant instability in river bridges, while mitigation measures such as increasing structural mass effectively reduce displacement and delay collapse [8]. Similarly, CFD analyses demonstrated that venting holes in T- and box-girder bridges reduces tsunami-induced uplift forces by releasing trapped air, thereby enhancing structural resilience [9].

Extensive research has been conducted on flood effects and debris impact on both traditional and pontoon-type floating bridges [10–12].

* Corresponding authors.
E-mail addresses: raizal@upm.edu.my (R.S. Muhammad Rashid), a.alameri@ku.edu.bh (A.Q. Al Ameri).

https://doi.org/10.1016/j.rineng.2026.112141
Received 12 October 2025; Received in revised form 6 March 2026; Accepted 22 July 2026
Available online 23 July 2026

However, these structural systems exhibit inherent functional limitations. Pontoon-type floating bridges are well suited for deep-water locations and can accommodate hydraulic forces induced by currents and floods. Nevertheless, they require large volumes of buoyant elements for construction and maintenance and may obstruct ship navigation due to their permanent placement [13]. Traditional bridges, on the other hand, allow uninterrupted navigation under normal conditions but are highly vulnerable during floods, often becoming fully submerged. Such sudden submergence poses severe safety risks to users and surrounding communities [14]. Moreover, traditional bridges are particularly susceptible to intense hydraulic forces and debris accumulation during flood events [15]. Debris transported by floodwaters plays a critical role in amplifying hydrodynamic loads and inducing localized stress concentrations on bridge components, significantly increasing the likelihood of structural damage or failure [12].

In this study, a semi-floating bridge refers to a bridge system that behaves as a conventional fixed structure under normal service conditions but transitions into a temporarily buoyant state during extreme flood events. Unlike fully floating pontoon bridges, the semi-floating concept preserves structural continuity and serviceability while reducing prolonged submergence, debris accumulation, and excessive shear demand during floods. Despite these potential advantages, existing studies predominantly focus on fixed bridges subjected to hydrodynamic loading or fully floating bridge systems. The shear response, failure mechanisms, and effectiveness of semi-floating UHPC box-girder bridges under combined flood flow and debris impact remain largely unexplored, particularly for girders without web shear reinforcement. This knowledge gap highlights the necessity of investigating semi-floating bridge systems to improve flood resilience and structural safety.

To address these challenges, this research proposes a semi-floating ultra-high-performance concrete (UHPC) box-girder bridge that integrates the functional advantages of traditional and pontoon bridge systems with the superior mechanical properties of UHPC. Under normal service conditions, the bridge functions as a conventional fixed structure, while during extreme floods it transitions into a floating configuration. This conditional buoyancy reduces prolonged submergence, limits debris accumulation, and mitigates excessive shear demand on structural components. To investigate this concept, a 1:7.5 scaled-down UHPC box-girder bridge model was used for both experimental testing and numerical simulations. UHPC, characterized by high compressive strength exceeding 120 MPa and tensile strength greater than 10 MPa, enables the elimination of conventional web shear reinforcement, thereby simplifying construction and enhancing durability [16–18]. Accordingly, this study evaluates the shear performance of the proposed bridge system under flood loading both with and without debris through a combined experimental and numerical investigation. This focus is particularly important, as flood-borne debris is widely recognized as a dominant contributor to excessive shear stresses that can trigger structural failure.

Recent literature has highlighted the critical role of debris in flood-induced bridge failures through both experimental and numerical investigations. Anisha et al. [19] reported that incorporating debris impacts into fragility curves for reinforced concrete bridges increased the probability of failure by up to 80% at a flood velocity of 6.8 m/s. Similarly, Friedl et al. [20] showed that horizontal loads acting on bridge superstructures typically range from one-fifth to three-fifths of the total debris-flow drag force. Qiu et al. [21], through flume experiments with flow velocities between 0.75 m/s and 6.14 m/s, observed a substantial increase in impact forces, reaching 74.76 kPa at the highest velocity. Kabir et al. [22,23] demonstrated that bridge geometry and debris-induced flow blockage significantly influence drag force evolution and overall hydrodynamic loading. Hasanpour et al. [24] numerically simulated tsunami-induced debris impacts on bridges and revealed that debris-related loads were approximately 2.67 times greater than those without debris. Fan et al. [25] showed that impact loads on reinforced concrete bridge piers increase proportionally with impact energy during barge collisions. By coupling discrete element methods with computational fluid dynamics, Jin et al. [26] reported that debris-laden flows can increase loads on bridge piers by up to 295%. Nan et al. [27] observed a sharp rise in structural stress from 20,000 Pa to 230,000 Pa in debris-free current flow simulations, while Wang et al. [28] demonstrated that pontoon-supported floating bridges are highly sensitive to collision-induced motions that significantly affect shear demand.

In summary, there is a clear need for a bridge system that functions as a conventional fixed structure under normal conditions while transitioning into a floating configuration during extreme flood events. The pronounced influence of debris-laden flow on shear demand must be explicitly considered in such designs. This study therefore introduces a semi-floating UHPC box-girder bridge without shear reinforcement that can float during floods while maintaining adequate shear resistance under combined flow and debris loading. The primary innovation of this study lies not merely in the use of UHPC, but in the development of an adaptive semi-floating bridge system with conditional buoyancy that fundamentally differs from both conventional fixed bridges and fully floating pontoon systems. Unlike previous research, the proposed framework integrates debris-aware hydrodynamic load quantification with a coupled computational strategy in which CFD-derived flow and debris forces are directly transferred into a structural finite element model for shear assessment. This multi-physics methodology enables, for the first time, a systematic evaluation of the shear behavior of UHPC box girders without web reinforcement under combined flow and debris loading. These contributions collectively establish a new conceptual and analytical basis for the design of flood-resilient bridge systems. To achieve the objectives of this study, a systematic approach was adopted, combining experimental and numerical investigations to evaluate the shear performance of the semi-floating UHPC box-girder bridge. The specific goals were:

(1) To conduct experimental tests on a semi-floating UHPC box-girder bridge prototype in a hydraulic laboratory under controlled flow, debris, and combined flow–debris conditions to measure reaction shear forces.
(2) To perform CFD simulations to evaluate floating behavior and quantify hydrodynamic drag forces at velocities up to 16 m/s for flow-only, debris-only, and combined loading scenarios.
(3) To apply CFD-derived distributed forces to a structural finite element model in ANSYS to accurately simulate shear response along the bridge girders.
(4) To assess the shear performance of UHPC box girders without web reinforcement under combined flow and debris loading, integrating experimental and numerical results for model validation.

This integrated and structured methodology enables a clear evaluation of shear failure mechanisms in semi-floating UHPC bridges, providing a new conceptual and analytical framework for the design of flood-resilient bridge systems.

2. Experimental and Theocratical Framework

2.1. Proposed Geometrical Model

The bridge geometry features small-scale dimensions at a 1:7.5 scale, simulating a real reinforced concrete bridge located in Perak, Malaysia. Fig. 1 presents the dimensions of the proposed box girder bridge in millimeters, with slight modifications to enhance flow resistance. The overall width of the cross-section is 1300 mm, with a total height of 286 mm in this study. The top slab thickness is 20 mm on both sides, while the bottom slab is 15 mm thick. The webs are spaced 412 mm apart. Each junction between the webs and bottom slab includes a curved fillet with a radius of 186 mm, forming a U-shaped contour for the bottom

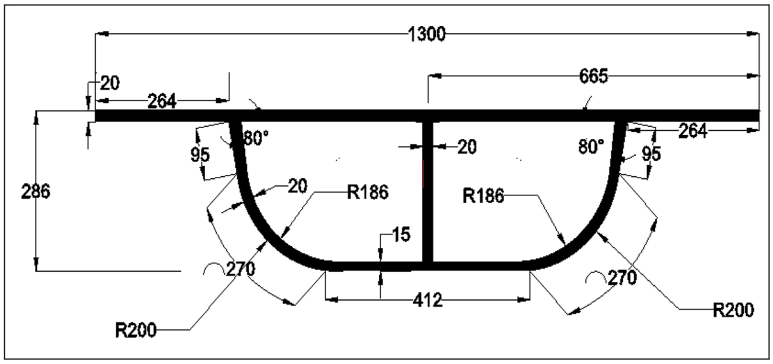

Fig. 1. Geometry of the proposed box girder bridge model.

cell. Notably, the corners near the outer edges are modified with a larger radius of 200 mm to enhance flow streamlining and reduce sharp stress concentrations. It can also be observed that angular transitions exist between the horizontal and vertical members. For instance, the side walls connect to the top slab at an angle of 80° and to the curved bottom fillets at 95°, which enhances structural integrity and promotes efficient force transfer. The inner vertical web has a thickness of 20 mm, while all horizontal members (top and bottom slabs) and outer webs maintain similar thicknesses, consistent with the thin-shell design principles of UHPC. Moreover, the bridge model was designed with a target compressive strength of 140 MPa at 28 days, a tensile strength of 15 MPa, an elastic modulus of 50 GPa, and a Poisson's ratio of 0.2. The debris used in the experiments measured 0.81 m × 0.35 m × 0.32 m and had a mass of 80 kg.

Moreover, the proposed bridge was tested for floating performance in the hydraulic laboratory at Universiti Putra Malaysia, as shown in Fig. 2. The bridge specimen was supported within a rectangular flume using two structural steel L-beams (75 × 75 mm) anchored to I-section piers (304 × 150 mm), ensuring lateral stability while allowing vertical flotation behavior, as illustrated in Fig. 2a. Three pressure sensors were installed along the front face and bottom surface of the bridge to capture time-dependent hydrodynamic pressure variations during flood flow and debris impact conditions. The bridge model was suspended by a central lifting hook to allow proper alignment and free vertical motion before testing. During the experiment, the inlet and outlet valves of the flume were kept open in each trial to simulate transient flood flow conditions as shown in Fig. 2b. This setup ensured the formation of a stable and consistent hydraulic front at the location of the floating bridge model. The presence of the bridge and its supporting structures did not obstruct flow development. All test scenarios, including both flow-only and debris impact cases, were repeated three times for durations of 60, 90, and 120 seconds to ensure repeatability and data reliability. The variation among repeated trials was within 5%, confirming good consistency and reproducibility of the experimental results. The results indicate successful floating of the proposed model with partial submersion, where only 120 mm of the model's depth was submerged

Fig. 2. Experimental setup of the floating bridge model: (a) model installation, (b) bridge submersion, and (c) flow and debris loading acting on the bridge.

(Fig. 2c). It is also interesting to note that the effects of flooding and debris impact were evaluated under maximum flow velocities of 0.5 m/s.

2.2. Computational Fluid Dynamics Model

The experimental flow velocity range was limited to 0.5 m/s due to laboratory flume capacity and safety considerations, while still providing reliable data for model validation. Higher velocities representative of extreme flood conditions were investigated numerically. The debris geometry and mass were selected based on scaled representations of commonly reported flood-borne debris such as timber logs and floating structural elements [30,33]. A numerical model was developed using computational fluid dynamics in ANSYS Fluent to simulate various flow conditions. The objective of this step was to predict the floating behavior of the proposed model with and without debris and to estimate the drag force generated by the water flow. The predicted drag force was later used as input for the developed finite element model (FEM) to investigate the shear resistance of the proposed bridge, which represents the main goal of this study as discussed in the next section.

Regarding the CFD model, the simulations employed the governing transport equations of the k–ω Shear Stress Transport (SST) turbulence model (ANSYS, 2017), as expressed in Eq. 1 and 2. In these equations, k and ω denote the turbulent kinetic energy and the specific turbulent dissipation rate, respectively. The terms G_k and $G\omega$ represent the generation of k due to velocity gradients and the production of ω. The terms Γ_k and $\Gamma\omega$ correspond to effective diffusivity, while Y_k and $Y\omega$ represent the dissipation of k and ω, respectively. Additionally, $D\omega$ denotes the cross-diffusion term, and S_k and $S\omega$ are user-defined source terms. The subsequent steps were adopted to develop the CFD model. First, the bridge model was created in CAD software and then imported into ANSYS Design Modeler. A 2D domain containing the bridge and debris was generated, followed by meshing. The mesh size ranged from 25 mm in regions near the boundary to 80 mm in regions farther away (Fig. 3a). A tetrahedral mesh was employed for both the bridge and debris to improve efficiency. Mesh quality metrics, including minimum orthogonal quality, aspect ratio, and skewness, were carefully evaluated before initializing the numerical models. The boundary conditions implemented in the numerical simulations are shown in Fig. 3b. At the inlet, a uniform velocity profile was prescribed with a constant water depth determined from the specified Froude number of 0.15. The top surface of the computational domain was subjected to atmospheric pressure. An open channel boundary condition with variable water depth was applied at the inlet, while the outlet was set as a pressure boundary. The channel bed and the bridge were modeled as wall boundaries with a no-slip condition and default roughness parameters. Near-wall treatment for turbulence was handled using the standard wall function.

$$\frac{\partial(\rho k)}{\partial t}+\frac{\partial(\rho k ui)}{\partial xi}=\frac{\partial}{\partial xi}\left(\Gamma k\frac{\partial k}{\partial xi}\right)+Gk+Yk+Sk \tag{1}$$

$$\frac{\partial(\rho\omega)}{\partial t}+\frac{\partial(\rho\omega ui)}{\partial xi}=\frac{\partial}{\partial xi}\left(\Gamma\omega\frac{\partial\omega}{\partial xi}\right)+G\omega+Y\omega+D\omega+S\omega \tag{2}$$

Furthermore, the Volume of Fluid (VOF) multiphase water–air model coupled with the k–ω SST turbulence model was employed in this study to account for turbulence effects, as illustrated in Fig. 4. The dynamic mesh feature, in conjunction with the six degrees of freedom (DOF) model, was used to simulate the bridge's dynamic response. The six DOF properties included a bridge mass of 190.620 kg with translation in the y-direction and a debris mass of 80 kg with translation in the x-direction. To avoid divergence issues, the time-step size was set to 0.001 s, following the Courant number criterion (less than 1) to ensure numerical stability. Twenty iterations per time step were performed to minimize the residuals of the x-, y-, and z-velocity components and the continuity equation. The convergence criterion for continuity and turbulence parameters was set to 10^{-6}. Pressure–velocity coupling was applied to solve the governing equations. The mathematical model for the fluid dynamics simulations consisted of the Navier–Stokes (N–S) equations, which describe the motion of an incompressible Newtonian fluid, coupled with the continuity equation for mass conservation. These equations were solved numerically using ANSYS (2017), as expressed in Eqs. (3–5). The velocity and pressure fields were strongly coupled, where velocity influenced pressure distribution and the pressure gradient affected velocity. A second-order upwind scheme was adopted to discretize momentum, turbulent kinetic energy, and the specific dissipation rate. To achieve better convergence, the under-relaxation factor for pressure was set at 0.30, while those for density, momentum, turbulent kinetic energy, and specific dissipation rate were set at 0.70. The drag force, lift force, and total pressure (static and dynamic) were monitored across all scenarios. The operating pressure was maintained at atmospheric conditions (101,325 Pa), while gravitational acceleration was applied in the y-direction at –9.81 m/s^2, with an operating density of 1.225 kg/m^3. Finally, the solution was initialized using standard initialization from the inlet.

$$\frac{\partial u}{\partial x}+\frac{\partial v}{\partial y}=0 \tag{3}$$

$$\frac{\partial u}{\partial t}+U\frac{\partial u}{\partial x}+V\frac{\partial u}{\partial y}+W\frac{\partial u}{\partial z}=-\frac{1}{\rho}\frac{\partial p}{\partial x}+v\left(\frac{\partial^2 u}{\partial x^2}+\frac{\partial^2 u}{\partial y^2}+\frac{\partial^2 u}{\partial z^2}\right)+Fx \tag{4}$$

$$\frac{\partial v}{\partial t}+u\frac{\partial v}{\partial x}+v\frac{\partial v}{\partial y}=-\frac{1}{\rho}\frac{\partial p}{\partial y}+v\left(\frac{\partial^2 v}{\partial x^2}+\frac{\partial^2 v}{\partial y^2}\right)+Fy \tag{5}$$

2.3. Structural modeling Model

After obtaining the drag forces from the CFD simulations, these forces were used as input for the structural analysis model developed in ANSYS to evaluate the effects of flow and debris on the shear performance of the proposed bridge model. Several steps were carried out to achieve this objective, beginning with importing the bridge geometry from CAD software, followed by defining material properties, generating

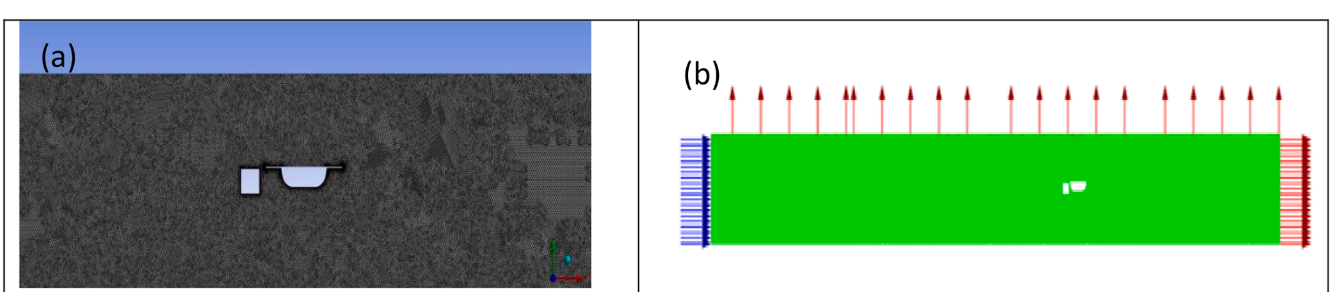

Fig. 3. Development of the CFD model: (a) meshing, (b) boundary conditions.

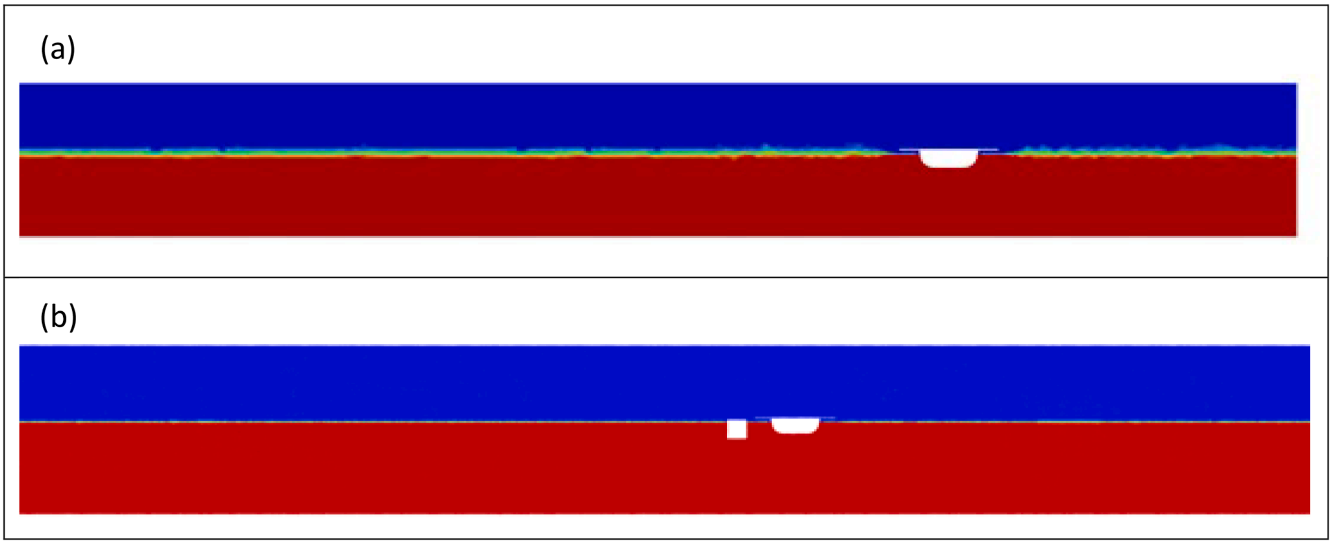

Fig. 4. Simulating the floating bridge model: (a) without debris (b) with debris.

the mesh, assigning boundary conditions, and applying loading and time-step settings. The bridge was modeled using triangular shell elements with a size of 25 mm, ensuring sufficient resolution to capture stress concentrations and impact interactions (Fig. 5). The mesh was further refined at contact regions to improve the accuracy of stress distribution predictions. Like CFD simulations, the structural analysis of the UHPC box girder bridge was conducted under two conditions: with debris impact and without debris. In both cases, hydrodynamic forces were applied to represent the effect of water flow acting on the bridge and debris at different velocities. For the debris-impact scenario, transient structural analysis was performed to capture the time-dependent reaction forces and stress distributions resulting from the collision between the debris and the bridge. Contact interactions were explicitly defined to simulate localized impact effects. In contrast, the non-debris scenario focused primarily on hydrostatic and hydrodynamic loading without direct impact. The UHPC material properties adopted in the structural model are summarized in Table 1. These parameters were derived from laboratory material testing conducted for the present study and supplemented by values reported in the literature for UHPC with comparable mechanical performance.

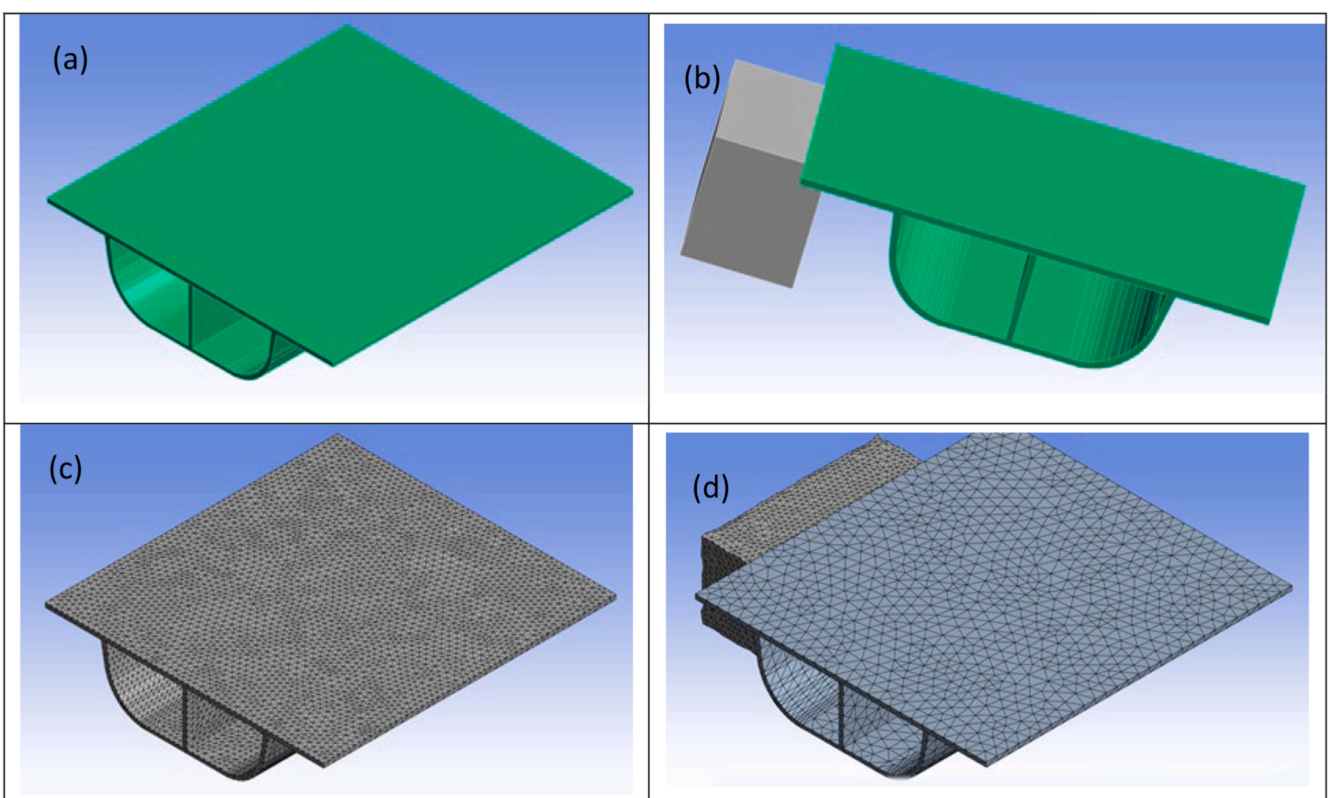

Fig. 5. Development of the structural shear response model: (a, b) geometry input with and without debris; (c, d) meshing for both cases.

Table 1
UHPC material parameters.

Property	Unit	Value
Compressive strength (f_{cube})	MPa	140
Elastic modulus (E)	GPa.	50
Poisson's ratio	—-	0.20.
Density (γ)	kN/m³.	25

2.4. Shear Parameters Calculation

The shear failure of the proposed model was evaluated using a simple mathematical parameter, the shear failure index (SFI). The SFI is designed to assess the vulnerability of the floating bridge under various flood exposure conditions. It is defined as the ratio between the bridge's shear resistance capacity and the shear demand induced by flood and debris impact forces (Eq. 6), where V_{Rd} represents the shear resistance capacity of the bridge girder and V^* denotes the shear induced by flood and debris impacts.

$$SFI = \frac{V_{Rd}}{V^*} \tag{6}$$

The shear resistance capacity of the bridge (V_{Rd}) was determined in accordance with the French standard (Eq. 7). In this context, $V_{Rd,c}$, $V_{Rd,s}$, and $V_{Rd,f}$ represents the design shear resistance provided by UHPC, steel stirrups, and steel fibers, respectively. Since no stirrups were used in the UHPC girder, $V_{Rd,s}$ was taken as zero. The value of $V_{Rd,c}$ was calculated using Eq. 8. A material safety factor (γ_{cfyE}) of 1.5, b_w of 20 mm and compressive strength of ($f_{ck,UHPC}$=120 Mpa) were adopted, while z was taken as $0.9 \times d$, where $d = 1950$ mm is the effective depth of the section. Furthermore, the coefficient k was determined using Eq. 9. With σ_{cp} equal to zero(no prestress), the shear resistance provided by steel fibers ($V_{Rd,f}$), it was calculated using Eq. 10, where A_{fv} denotes the effective vertical web area, θ is the angle of inclination of the principle compression stress to the longitudinal axis (taken as $\theta = 30^o$), and $\sigma_{Rd,f}$ is the design value of the post-cracking tensile strength, obtained using $K = 1.25$ and $\gamma cf = 1.25$, also defined as Eq. 11.

$$V_{RD} = V_{Rd,c} + V_{Rd,s} + V_{Rd,f} \tag{7}$$

$$V_{Rd,c} = \left(0.24 \Big/ \gamma_{c\,f_y\,E}\right) k f_{ck,UHPC}^{1/2}\, b_w\, z \tag{8}$$

$$k = 1 + 3\sigma cp \Big/ f_{ck,UHPC} \tag{9}$$

$$V_{Rd,f} = A_{fv}\sigma_{Rd,f}\cot\theta \tag{10}$$

$$\sigma_{Rd,f} = f_{ct,fk} \Big/ K.\gamma_{cf} \tag{11}$$

Regarding the shear induced by flood and debris impacts (V^*), its value varies depending on the type of loading, including water flow only, debris impact, or their combined action. The influence of shear force variations was evaluated in the ANSYS model for different flood velocities ranging from 0.5 m/s to 16.0 m/s, in increments of 0.5 m/s for flow without debris, and at 7.0 m/s for flow with debris impact. Separate simulations were carried out to isolate the effects of flood flow and debris impact.

3. Results and Discussion

3.1. Hydrodynamic Drag Force Analysis

This section presents the predicted drag force obtained from the CFD model for the proposed floating bridge under various flow velocities, both with and without debris. Analyzing hydrodynamic forces is crucial for assessing the vulnerability of the bridge superstructure to flooding Kabir, et al. [22]. In this study, the relationship between drag force and velocity is shown in Fig. 6. The results indicate that the drag force increases with velocity in both scenarios, which is consistent with hydrodynamic theory, where drag force is proportional to the square of velocity. However, the degree of influence varies according to the contribution of debris. For instance, in the absence of debris, the increase in drag force is gradual and relatively smooth across the entire velocity range, from 0.5 m/s up to 16 m/s, indicating stable hydrodynamic resistance behavior. In contrast, in the presence of debris, the drag force increases more sharply and nonlinearly starting from around 3.5 m/s, reflecting significant amplification due to debris accumulation. Sudden jumps in drag force (notably around 4.5–5.5 m/s and again at 6.5–7.0 m/s) suggest complex interactions between debris and the flow, such as debris impacting or obstructing the flow near the bridge body. At 7.0 m/s with debris, the drag force reaches approximately 45,000 N, whereas the same magnitude of drag force is only reached at about 15.5 m/s without debris. These findings confirm the significant role of debris in increasing drag force on the bridge, particularly at higher velocities, which is consistent with observations reported in previous studies.

It should be noted that, in ANSYS, the flow-induced drag was applied as a uniformly distributed load along the bridge web, while debris impacts were applied as concentrated loads at the contact points. The CFD-predicted magnitudes were used directly in both cases, allowing the structural model to respond realistically to steady and fluctuating forces and accurately capture shear stresses under different flow conditions and debris impacts.

In addition, the drag force behavior was analyzed at velocities of 0.5 m/s, 3.5 m/s, and 7.0 m/s under flow-only conditions (Fig. 7) and with debris (Fig. 8), the drag force increases with velocity following the expected quadratic relationship, while the interaction time between the flow and the bridge web decreases from approximately 0.04 s at 0.5 m/s to 0.016 s at 3.5 m/s and 0.014 s at 7.0 m/s. In contrast, when debris is present, the drag force becomes more irregular and dynamic, with delayed impact times of about 1.3 s at 0.5 m/s, 0.225 s at 3.5 m/s, and 0.11 s at 7.0 m/s, as shown in Fig. 8. This delay is attributed to the inertia and mass of the debris, which resists acceleration from the surrounding fluid before transferring force to the bridge web. Upon impact, the drag force response becomes highly fluctuating and turbulent, unlike the smoother and earlier steady-state behavior observed in flow-only cases. These results highlight that debris not only amplifies the drag force but also alters its timing and stability, underscoring the need to account for debris-induced loads in the structural design and safety assessment of floating bridges.

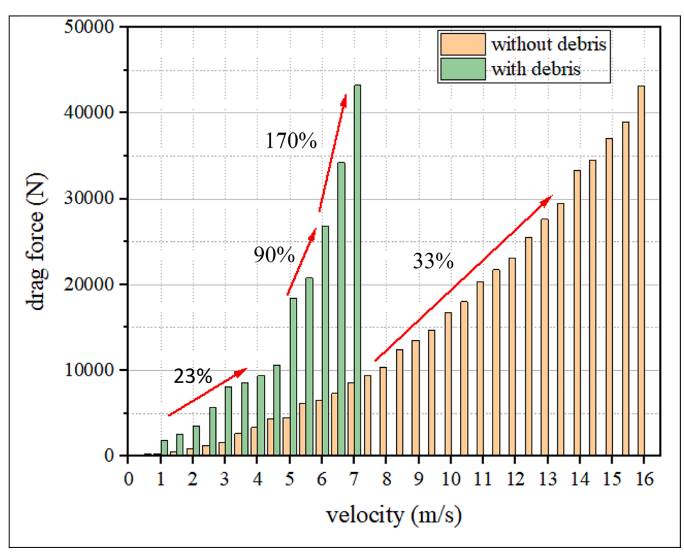

Fig. 6. Comparison of drag force under different flow velocities with and without debris.

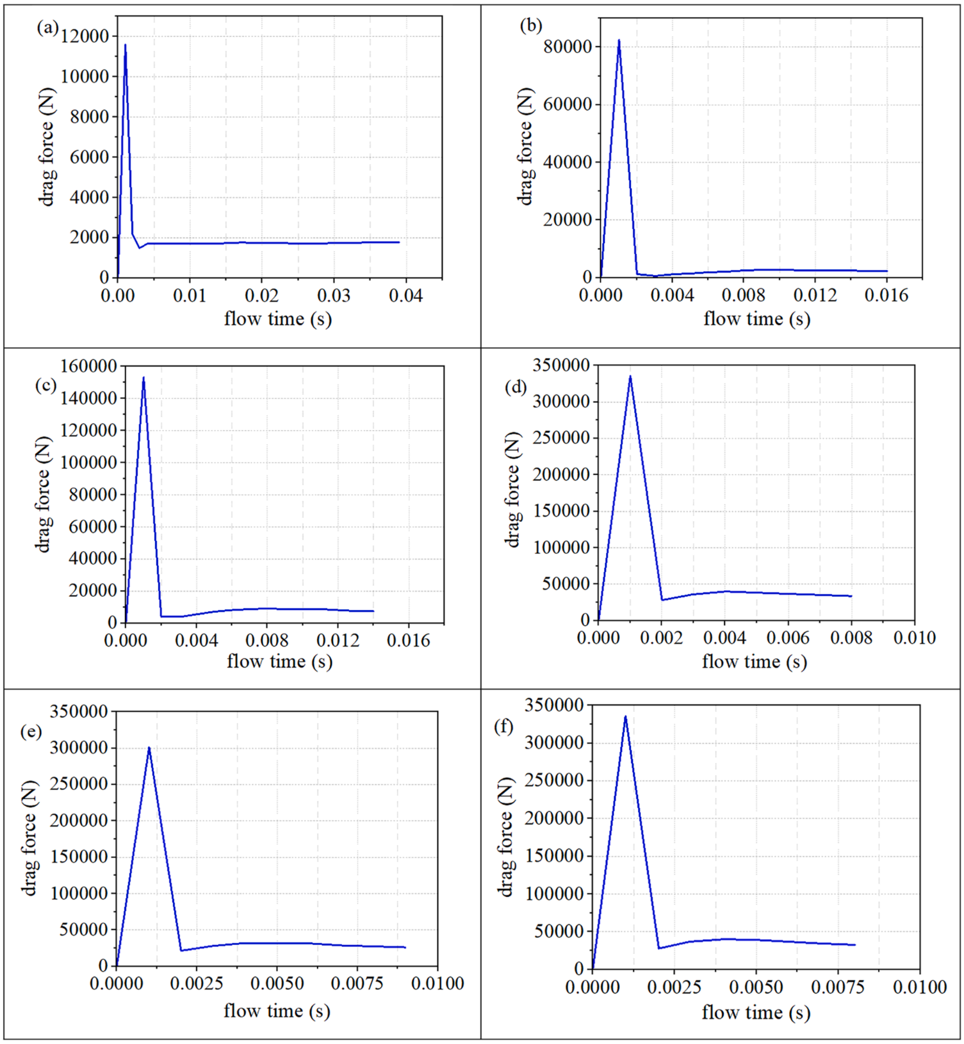

Fig. 7. Behavior of drag force at various velocities without debris at (a) 0.5m/s, (b) 3.5m/s, (c) 7.0m/s (d) 10 m/s (e) 13 m/s, and (f) 16 m/s.

3.2. Structural Response Under Hydrodynamic Loading and Debris Impact

In this section, the structural response of the bridge model subjected to hydrodynamic loading and debris impact was systematically investigated, with particular focus on shear stress. The analysis was carried out in two sequential stages. In the first stage, the shear force at the bridge support, identified as the critical location experiencing the maximum force, was quantified and examined. In the second stage, the corresponding shear stress at the same location was evaluated to provide a comprehensive understanding of the bridge's performance under these loading conditions.

It is interesting to note that the analysis was conducted under three distinct scenarios: flow loading alone V_{flow}, debris loading V_{debris}, and the combined action of flow and debris $V_{\text{flow+debris}}$. Fig. 9 presents the shear force responses under these conditions. The results show distinct behaviors and magnitudes across the three scenarios. Under flow-only loading, the shear force increased gradually at velocity, reaching a maximum of approximately 3200 N at 15.5 m/s. In contrast, the inclusion of debris produced sharp increments in shear force at relatively low velocities, highlighting its significant influence on structural performance. For instance, under the combined flow and debris scenario, the maximum shear force of nearly 25,000 N was recorded at only 4 m/s. These findings emphasize the critical importance of accounting for both flow and debris forces in the structural assessment of floating bridges subjected to extreme flood conditions to capture the true shear demand.

A similar trend was observed for the shear stress evolution at local response under the three loading conditions, as illustrated in Fig. 10. The results demonstrate that shear stress increases with velocity in all cases. Under flow-only conditions, a gradual rise in $\tau_{\max}$ was observed, increasing from approximately 1 MPa at 0.5 m/s to 4.5 MPa at 3.5 m/s. Under debris impact, higher shear stresses were recorded compared to the flow-only case, particularly at elevated velocities. Furthermore, the combined loading condition (flow + debris) produced the highest shear stress across all velocities, reaching up to 11 MPa at 3.5 m/s. This behavior highlights the cumulative and nonlinear influence of debris on the structural shear response, reinforcing the necessity of incorporating debris effects in flood load assessments. A deeper analysis of local shear failure shows that while flow alone produces relatively uniform stresses along the web, debris impacts generate localized stress concentrations, and combined loading amplifies these peaks. Considering these local variations provides a more complete understanding of the box girder's vulnerability under realistic flood and debris conditions.

The spatial distribution of local maximum shear stresses under debris impact is illustrated in Fig. 11. At a low flow velocity of 0.5 m/s (Fig. 11a), the stress concentrations are relatively small and localized, mainly occurring near the junctions of the bottom slab and vertical webs, indicating limited shear demand in these regions. As the velocity increases to 3.5 m/s (Fig. 11b), the contour plots show a noticeable increase in stress magnitude along the midspan region of the bottom slab

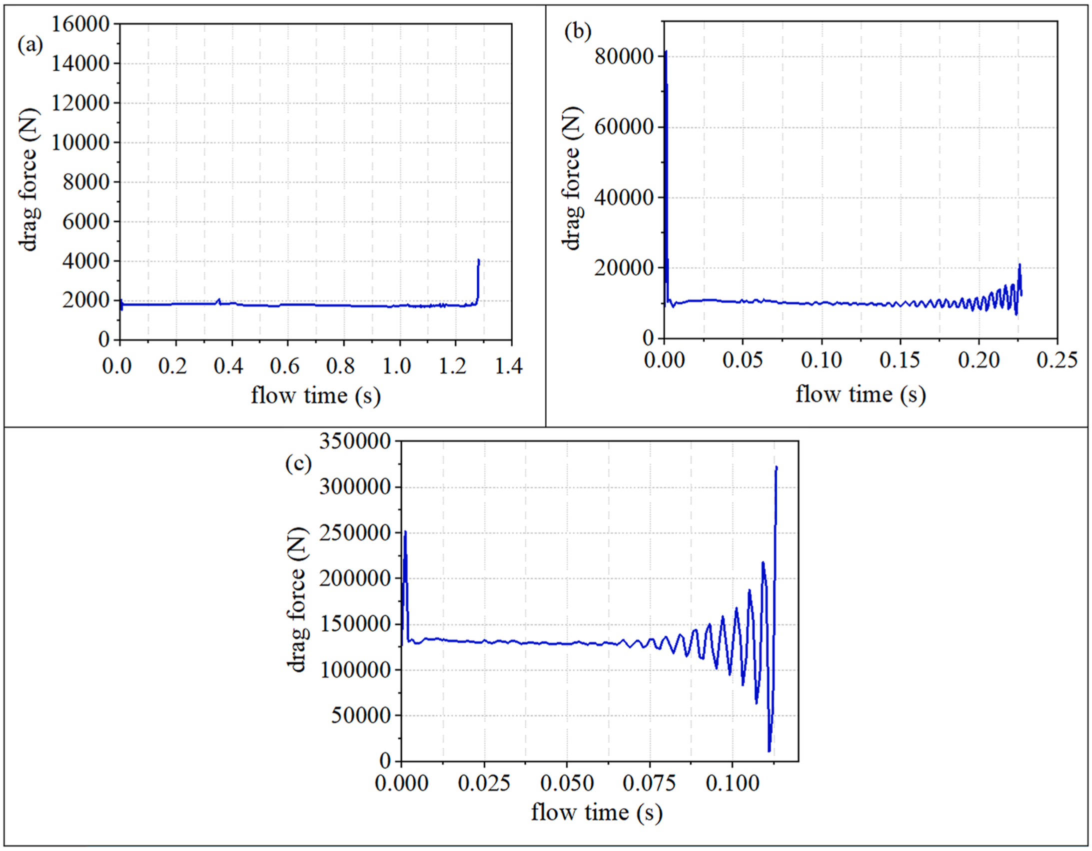

Fig. 8. Behavior of drag force at various velocities with debris at (a) 0.5m/s, (b) 3.5m/s, (c) 7.0m/s.

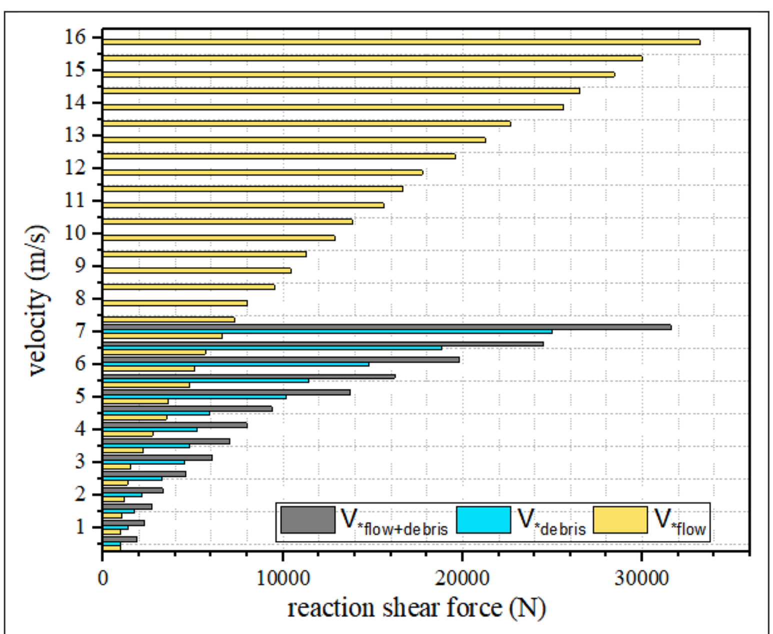

Fig. 9. Variation of reaction shear force under flow loading-only, debris loading, and combined loading conditions.

and the inner surfaces of the webs, suggesting higher local shear forces caused by intensified debris collision and increased hydrodynamic pressure gradients. At the highest simulated velocity of 7.0 m/s (Fig. 11c), the stress concentrations become significantly more pronounced and extend over larger regions, particularly near the corner zones of the box-girder cross-section and along the shear-critical web areas close to the supports, which are potential initiation points for local shear failure. The contour plots also indicate that the stress distribution is highly non-uniform along both the length and depth of the girder, with localized maxima occurring where debris impact coincides with flow-induced vortices and geometric discontinuities. These results highlight the combined influence of hydrodynamic loading, debris momentum

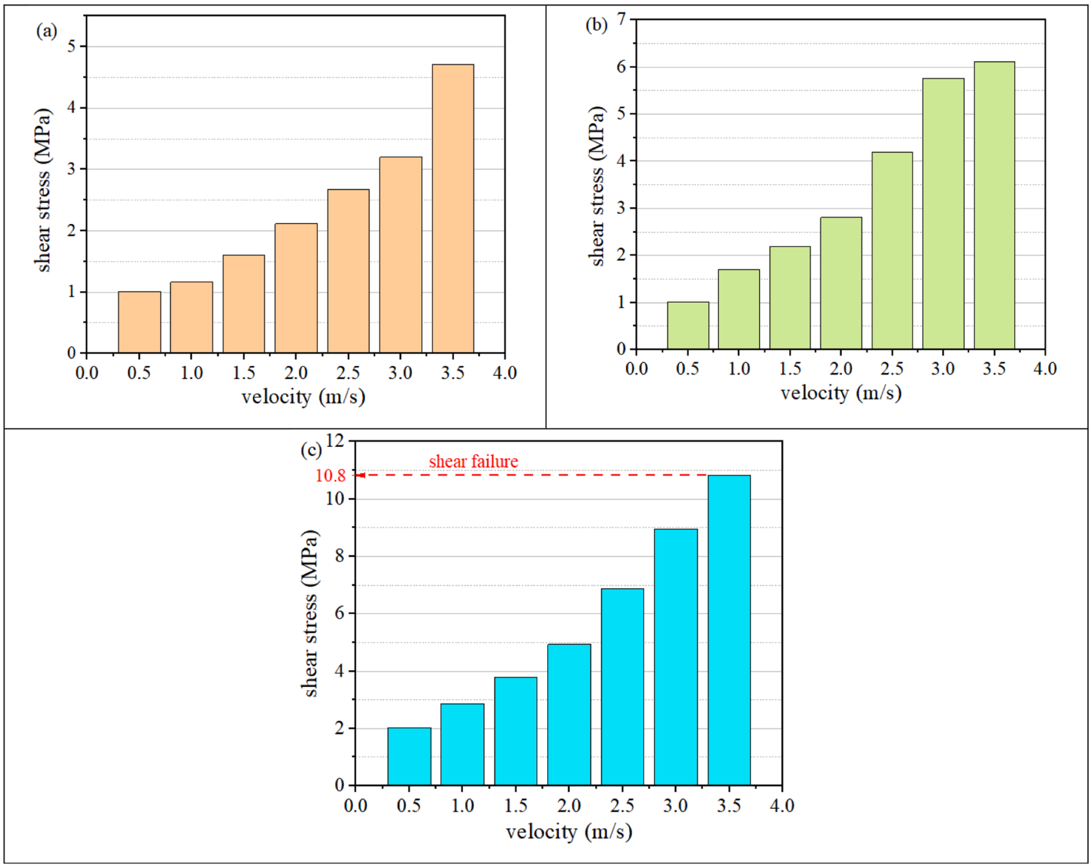

Fig. 10. Evolution of shear stress (a) flow loading-only, (b) debris loading, and (c) combined loading conditions.

transfer, and structural geometry in governing the shear response of the floating UHPC box-girder bridge.

3.3. Shear Failure Analysis

After obtaining the predicted shear stress on the web of the box girder bridge at the support, the potential for shear failure was evaluated using a mathematical parameter known as the shear failure index (SFI). This parameter was used as a baseline to identify the corresponding flow velocity at which shear failure could occur under three scenarios: (a) hydrodynamic loading-only, (b) debris loading, and (c) combined loading conditions. When the SFI approaches a value of one, it indicates that the shear capacity of the UHPC bridge is nearly equal to the shear demand induced by the applied loading scenario. Conversely, values greater than one signify that the bridge possesses sufficient shear capacity to resist the imposed forces, suggesting enhanced safety against shear failure.

Figure 12 illustrates the relationship between SFI and flood velocity, providing critical insights into the structural response under varying impact conditions. The results reveal a consistent trend in which SFI values decrease as flood velocity increases, reflecting a reduction in the structural safety margin as shear demand intensifies.

Under flow-only conditions, the critical velocity corresponding to shear failure is approximately 15.5 m/s, representing the maximum flood flow the bridge can sustain before reaching its shear limit. When debris loading is introduced, the critical velocity is significantly reduced to around 7.0 m/s, indicating that the presence of debris dramatically amplifies local shear stresses and decreases the global shear capacity of the structure. This reduction clearly demonstrates that debris is a dominant factor in limiting the safe operational velocity of the UHPC floating bridge. When flood flow was combined with debris impact, moderately lower SFI values were observed, suggesting that debris alters the load distribution and partially influences the overall shear response. In contrast, localized debris-induced shear failure produced the lowest SFI values, underscoring that while debris can cause concentrated damage, its effect on global structural vulnerability remains more localized. These logarithmic vulnerability curves highlight the importance of accounting for flood-induced shear effects and debris impact in bridge design. A clear understanding of these trends is essential for risk assessment and mitigation planning, thereby enhancing the resilience of UHPC floating bridges under extreme hydrodynamic conditions.

The shear failure distribution of the semi-floating UHPC box-girder bridge was further analyzed under varying flow conditions. Fig. 13 illustrates the shear stress contours at 7.0 m/s for (a) flow-only and (b) combined flow–debris loading scenarios. The results indicate that the presence of debris significantly amplifies the shear demand, particularly along the bottom slab and web intersections.

3.4. Comparative Evaluation of the Proposed Bridge Model

The results demonstrate a clear difference between hydrodynamic drag forces generated by flood flow alone and those amplified by debris impact on the UHPC floating bridge. At a low flood velocity of 0.5 m/s, the drag force under flow-only conditions was approximately 54 N, whereas debris impact increased the force to 292 N, a 4.7-fold amplification. With increasing velocity, this amplification trend remained consistent: at 2.5 m/s, drag rose from 1250 N to 5000 N; at 5 m/s, from 5000 N to 20,000 N; and at 7 m/s, from 8500 N to 43,250 N, representing a 5.1-fold increase. These findings indicate a recurring pattern where debris substantially intensifies loading, particularly on the webs of the bridge, which are most susceptible to concentrated shear stresses. This observation is in line with Luo, et al. [29] and Hasanpour, et al. [24], who reported that debris collisions can elevate impact pressures on bridge superstructures by three to five times relative to hydrodynamic

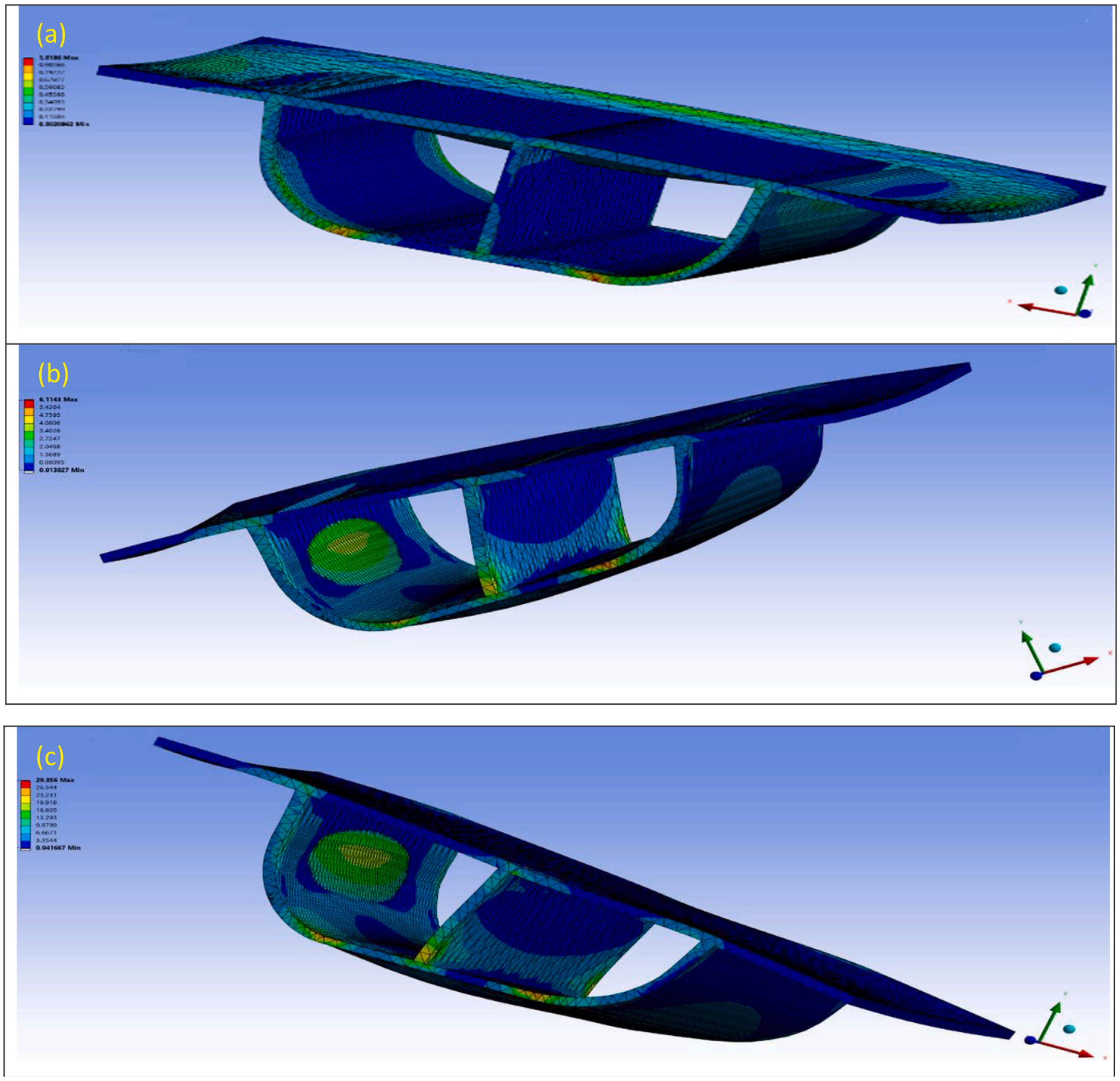

Fig. 11. Local maximum shear stress distribution in the semi-floating UHPC box-girder bridge under debris impact at flow velocities of (a) 0.5 m/s, (b) 3.5 m/s, and (c) 7.0 m/s.

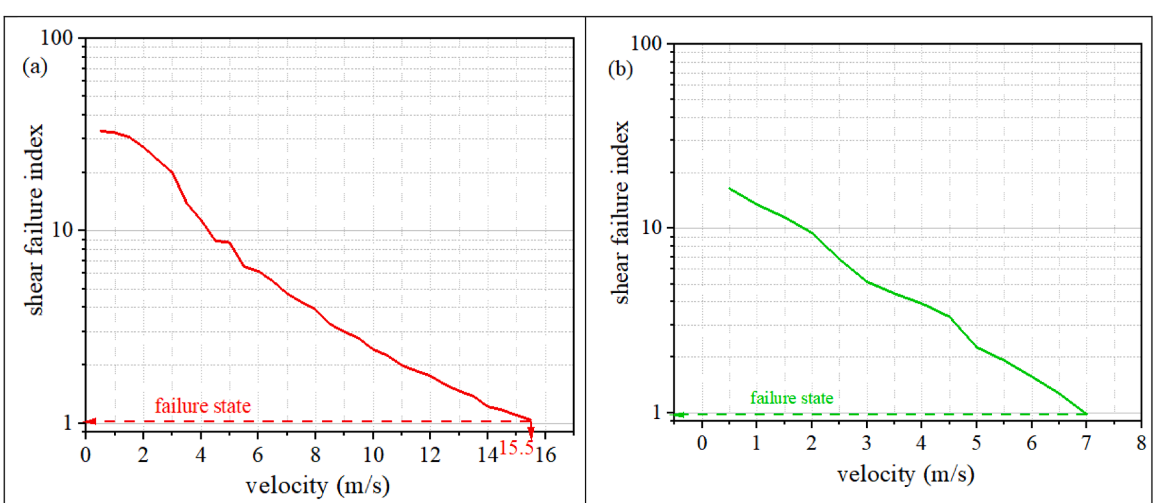

Fig. 12. Logarithmic vulnerability curves using shear failure index (a) flow loading-only, (b) debris loading, and (c) combined loading conditions.

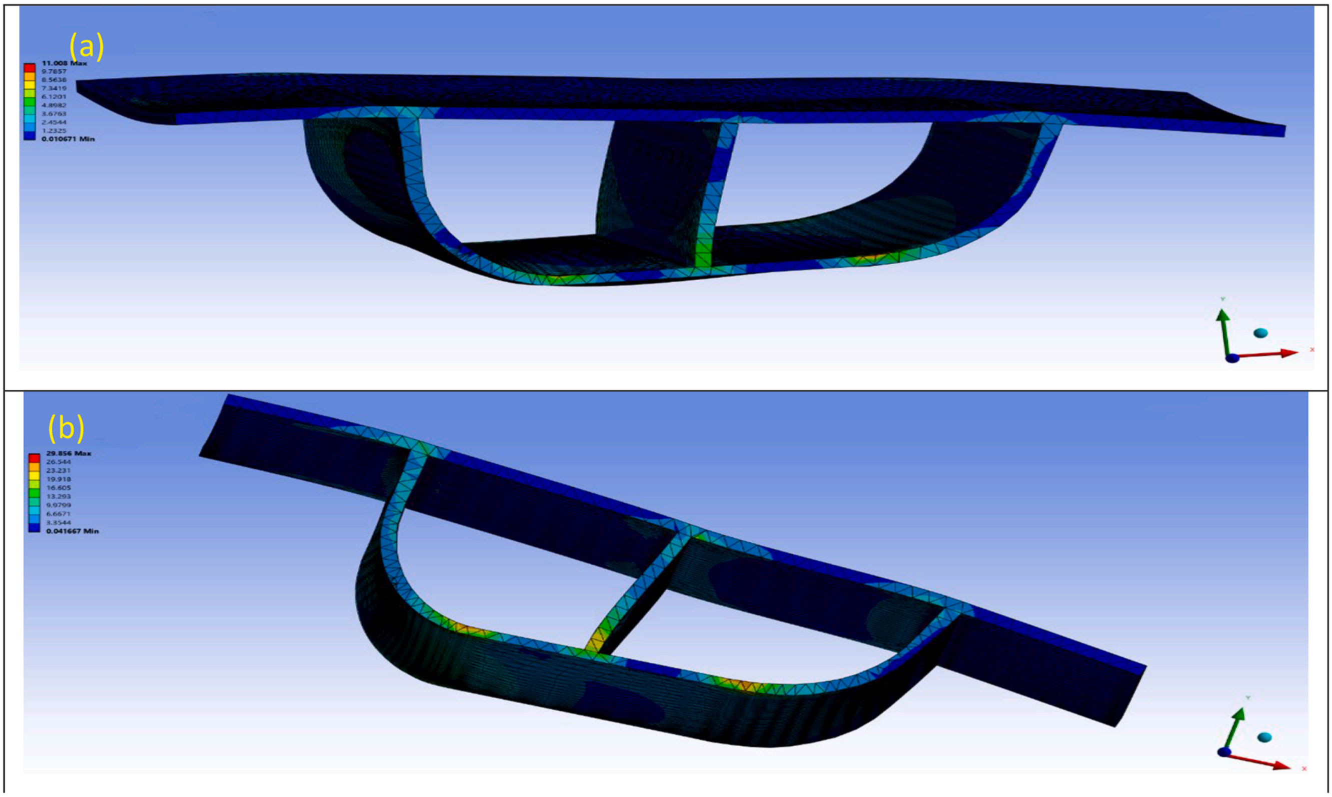

Fig. 13. Shear failure distribution of the semi-floating UHPC box-girder bridge at 7.0 m/s under (a) flow-only and (b) combined flow–debris loading conditions.

flow alone, with peak intensities during initial collision and rebound phases. The present study extends these findings by offering quantitative evidence that highlights the necessity of considering debris-induced effects in floating bridge design, particularly under extreme flood conditions.

In addition to drag force amplification, the variation of the shear failure index (SFI) across flood velocities further illustrates the influence of debris on structural response. Under flow-only conditions, the UHPC floating bridge-maintained stability up to approximately 16 m/s. When debris was introduced, however, the failure velocity was reduced to about 7 m/s, reflecting the increased shear demand and reduced tolerance under impact loading. While Kalendher, et al. [30], reported allowable flood velocities of only 3.66 m/s for prestressed concrete girder bridges under flow-only conditions and 0.89 m/s under debris impact, it is important to note that their study involved conventional concrete with lower compressive strength and without UHPC enhancements. Therefore, although not directly comparable in terms of material properties and structural configuration, this comparison provides a useful benchmark, emphasizing the superior performance of UHPC in sustaining both hydrodynamic and debris-induced loads. This enhanced performance is attributed to UHPC's exceptional mechanical properties, including compressive strength exceeding 120 MPa, tensile capacity over 10 MPa, and the efficiency of the box-girder geometry in resisting both localized and global failure mechanisms. These factors collectively enable the UHPC floating bridge to tolerate higher flow velocities and significantly mitigate the impact of debris compared to conventional prestressed concrete systems.

To further quantify vulnerability, fragility curves were developed for three scenarios: flow-only, flow with debris, and local shear from debris (Fig. 14). These curves revealed distinct differences in structural fragility across impact conditions. At a representative velocity of 6.8 m/s, the probability of failure remained negligible under flow-only conditions but increased to nearly 30% with debris impact. When compared with the findings of Anisha, et al. [19], who reported an 80% failure

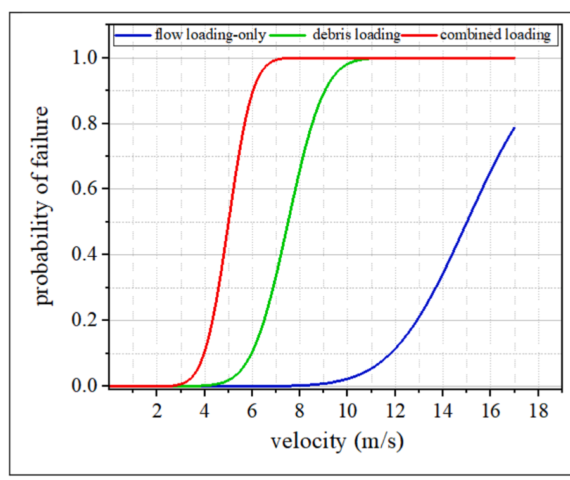

Fig. 14. Fragility assessment under progressive flood velocities and debris impact scenarios.

probability for reinforced concrete bridges under debris impact at the same velocity, the UHPC box-girder bridge demonstrated considerably greater resilience. This comparison further reinforces that the UHPC bridge configuration provides a robust solution for extreme flood events, highlighting its improved structural reliability over conventional designs.

Taken together, these findings demonstrate that UHPC floating bridges not only provide superior resistance to hydrodynamic drag and debris impact but also exhibit markedly lower fragility than conventional reinforced concrete systems. Consequently, UHPC offers a robust and resilient solution for floating bridge applications in flood-prone regions, where combined flow and debris loading govern structural safety.

3.5. Experimental Shear Force Validation

Experimental tests were conducted in a hydraulic flume under three loading scenarios: flow-only, debris-only, and combined flow–debris conditions, at a controlled flow velocity of 0.5 m/s (Fig. 2). For model validation, the reaction shear forces measured at the bridge supports in the experiments were directly compared with the corresponding numerical predictions obtained from the CFD–structural simulation framework, as described in Section 3.2. These reaction forces were selected as the primary validation parameter because they directly represent the global shear response of the bridge system under hydrodynamic and debris-induced loading.

Model validation was performed using the error percentage, a statistical indicator commonly used in experimental–numerical comparisons in structural and concrete engineering studies. The error percentage was calculated as the ratio of the difference between the experimental and predicted values to the experimental value, multiplied by 100. According to Algaifi et al. [31], predictive models exhibiting error percentages below 5% can be considered highly accurate, while Abdulkadir et al. [32] reported reliable numerical performance with error values up to 5.5%.

In the present study, the error percentage was consistently below 6%, confirming the accuracy and reliability of the developed numerical model (Fig. 15). Under the flow-only condition, the experimentally measured reaction shear force at the supports was 997.11 N, while the corresponding numerical prediction was 942 N. Similarly, for the debris impact scenario, the experimental shear force averaged 980 N, which closely matched the numerical value of 948 N. The close agreement between experimental measurements and numerical predictions indicates that the proposed modelling framework accurately captures the hydrodynamic loading and resulting structural shear response of the semi-floating UHPC box-girder bridge.

It should be noted that experimental validation at higher flow velocities (e.g., 16 m/s) could not be conducted due to hydraulic flume capacity and laboratory safety limitations. Therefore, numerical simulations were used to investigate extreme flood scenarios beyond the experimental range. Future research should incorporate large-scale or high-capacity experimental facilities to further validate the model under higher velocity conditions and improve predictive capability for extreme flood events.

4. Conclusion

This study introduces a novel ultra-high-performance concrete (UHPC) box girder bridge design with no shear reinforcement, capable of floating during flooding while maintaining exceptional shear resistance. The superior mechanical properties of UHPC, particularly its high tensile and compressive strength, enable the structure to withstand extreme hydrodynamic stresses. To achieve this, a series of steps were undertaken, including laboratory-scale compressive investigations and theoretical analysis using finite element methods. The proposed model was subjected to flow velocities ranging from 0.5 m/s to 16 m/s under three different loading conditions: (i) water flow only, (ii) debris impact only, and (iii) combined water flow and debris impact. Based on the study findings, several key points were drawn:

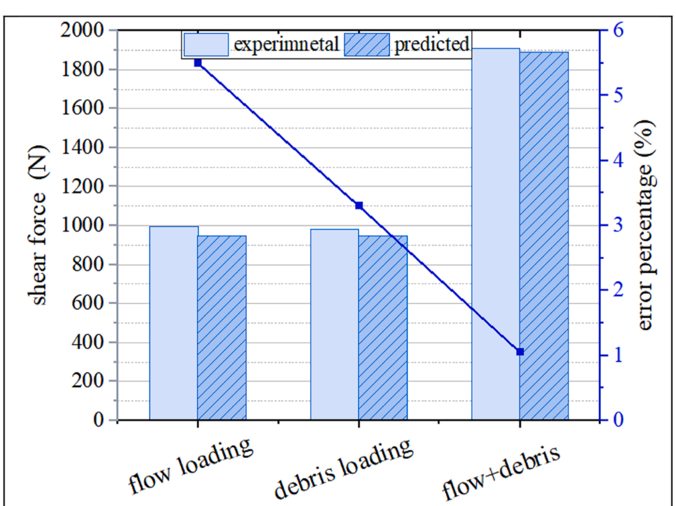

Fig. 15. Validation of the proposed model using absolute error percentage.

1) The proposed model successfully demonstrated floating capability under flooding conditions, providing an innovative solution for enhancing public safety and infrastructure resilience. In flume laboratory experiments, only 120 mm of partial submersion was recorded from the total depth, confirming the effectiveness of the design. This remarkable outcome encourages civil engineering researchers to move beyond conventional bridge functions—focused solely on structural or hydraulic loading—and consider temporary floating capacity under extreme flood conditions. Such an approach offers several benefits, including improved safety during floods and solutions to navigation challenges caused by pontoon floating bridges, which frequently obstruct shipping.
2) The computational fluid dynamics analysis confirmed that hydrodynamic drag forces increase proportionally with velocity, consistent with fundamental fluid–structure interaction principles. The proposed model withstood substantial drag forces under flow-only conditions, sustaining velocities up to 15.5 m/s without failure. This performance is attributed to the superior mechanical properties of UHPC, including a tensile strength of 15 MPa and a compressive strength of 140 MPa. However, debris impact significantly amplified drag forces, up to five times higher compared to flow-only scenarios, reducing the critical velocity threshold from 15.5 m/s to approximately 7.0 m/s. These results establish debris as the dominant factor influencing shear vulnerability.
3) The structural response obtained from the element modeling revealed that the proposed bridge-maintained shear stresses well below its shear capacity of 10.6 MPa under flow-only conditions. In contrast, debris loading generated localized stress concentrations on the webs, accelerating crack initiation and reducing the shear failure index. Critical shear failure index values were recorded at flow velocities of 16 m/s (flow-only), 7 m/s (debris-only), and 3.5 m/s (combined flow and debris). These findings demonstrate both the superior shear resistance of the UHPC box girder bridge and the critical influence of debris in reducing structural safety margins.
4) This research provides a pathway for future studies into flood-resilient bridge systems that integrate temporary floating capability with high shear resistance. The proposed concept presents a sustainable and innovative solution to the increasing challenges of climate change and global warming, particularly the rising frequency of severe flooding. Unlike pontoon floating bridges, this design avoids navigation obstructions, ensures smoother ship passage, and offers significant shear capacity against debris-induced flooding stresses. Furthermore, it provides valuable insights into the shear performance of UHPC box girder bridges without shear reinforcement, serving as a strong foundation for future exploration. Additional research is encouraged, particularly focusing on advanced fluid–structure interaction modeling, to refine design guidelines and enhance the development of flood-resilient UHPC bridges.
5) The findings have practical implications for bridge flood design. Debris-induced forces can greatly exceed current code assumptions, suggesting that design specifications could benefit from incorporating such effects, emphasizing UHPC use, and applying fragility-based assessments for performance-based evaluation. While further validation is required before revising codes, this study provides a

foundation for enhancing the resilience of floating bridges in flood-prone regions.

6) Despite the comprehensive analysis, this study has certain limitations. In particular, the effects of scale and the randomness of debris characteristics were not fully captured. Laboratory flume experiments and CFD simulations were performed at reduced scales and with idealized debris, which may not entirely represent real-world flood and debris interactions. Future work should consider full-scale testing and stochastic debris modeling to account for variability in debris size, shape, and impact location, thereby improving the reliability of the design guidelines.

Overall, the proposed UHPC floating bridge concept demonstrates superior shear resistance, floating capability, and resilience to combining flow and debris loading, offering a sustainable and innovative solution for flood-resilient infrastructure.

CRediT authorship contribution statement

Aso Abdulghafur Faqe Rahim: Writing – original draft, Visualization, Validation, Software, Methodology, Investigation, Formal analysis. **Raizal Saifulnaz Muhammad Rashid:** Supervision. **Nor Azizi:** Supervision. **Badronnisa Yusuf:** Supervision. **Adeb Qaid Al Ameri:** Funding acquisition. **Voo Yen lei:** Methodology, Resources, Supervision. **Hassan Amer Algaifi:** Writing – review & editing, Visualization.

Declaration of competing interest

The authors certify that they have NO affiliations with or involvement in any organization or entity with any financial interest (such as honoraria; educational grants; participation in speakers' bureaus; membership, employment, consultancies, stock ownership, or other equity interest; and expert testimony or patent-licensing arrangements), or non-financial interest (such as personal or professional relationships, affiliations, knowledge or beliefs) in the subject matter or materials discussed in this manuscript. Author names:

Acknowledgments

This research was partially funded by Kingdom University, Bahrain, under Research Grant No. KU-2025-2026-01.

Data availability

The data that has been used is confidential.

References

[1] D.K. Devendiran, S. Banerjee, A. Mondal, Impact of climate change on multihazard performance of river-crossing bridges: Risk, resilience, and adaptation, Journal of Performance of Constructed Facilities 35 (1) (2021) 04020127.
[2] A. Orcesi, et al., Investigating the effects of climate change on structural actions, Structural Engineering International 32 (4) (2022) 563–576.
[3] R.K. Arora, et al., Hydraulic Loads on Bridges during Floods: Comparative Assessment Based on Code Provisions, Journal of Structural Design and Construction Practice 30 (3) (2025) 04025059.
[4] G. Zhang, et al., Causes and statistical characteristics of bridge failures: A review, Journal of Traffic and Transportation Engineering (English Edition) 9 (3) (2022) 388–406.
[5] T. Ahamed, J.G. Duan, H. Jo, Flood-fragility analysis of instream bridges–consideration of flow hydraulics, geotechnical uncertainties, and variable scour depth, Structure and Infrastructure Engineering 17 (11) (2021) 1494–1507.
[6] S.A. Argyroudis, S.A. Mitoulis, Vulnerability of bridges to individual and multiple hazards- floods and earthquakes, Reliability Engineering & System Safety 210 (2021) 107564.
[7] Q. Fang, et al., Analysis of hydrodynamic forces acting on submerged decks of coastal bridges under oblique wave action based on potential flow theory, Ocean Engineering 169 (2018) 242–252.
[8] Z. Liu, et al., Investigation on flooding dynamic response and mitigation measure of river bridge, Engineering Failure Analysis 167 (2025) 1089.
[9] S. Niu, et al., CFD Analysis of tsunami impact and mitigation through venting holes in T- and box-girder, Ships and Offshore Structures (2025) 1–22.
[10] M. Kosič, L.J. Prendergast, A. Anžlin, Analysis of the response of a roadway bridge under extreme flooding-related events: Scour and debris-loading, Engineering Structures 279 (2023) 115607.
[11 M. Nasim, S. Setunge, Damage Estimation of a Concrete Pier When Exposed to Extreme Flood and Debris Loading, Journal of Marine Science and Engineering 10 (5) (2022) 710.
[12] M. Kosič, A. Anžlin, V. Bau', Flood Vulnerability Study of a Roadway Bridge Subjected to Hydrodynamic Actions, Local Scour and Wood Debris Accumulation, Water 15 (1) (2023) 129.
[13] Y. Sha, J. Amdahl, Numerical investigations of a prestressed pontoon wall subjected to ship collision loads, Ocean Engineering 172 (2019) 234–244.
[14] E. Majtan, L.S. Cunningham, B.D. Rogers, Experimental and Numerical Investigation of Floating Large Woody Debris Impact on a Masonry Arch Bridge, Journal of Marine Science and Engineering 10 (7) (2022) 911.
[15] S. Ji, et al., Dynamic response analysis of a floating bridge with bottom damaged opening based on the Kane method, Applied Ocean Research 154 (2025) 104365.
[16] J. Yang, et al., Experimental investigation and prediction of shear capacity for UHPC beams, Case Studies in Construction Materials 16 (2022) e01097.
[17] A. Standard, Standard practice for fabricating and testing Specimens of ultra-high performance concrete, ASTM International, West Conshohocken, PA, 2017.
[18] M. AlHamaydeh, M. Elkafrawy, S. Banu, Seismic Performance and Cost Analysis of UHPC Tall Buildings in UAE with Ductile Coupled Shear Walls, Materials 15 (8) (2022) 2888.
[19] A. Anisha, et al., Fragility functions for highway RC bridge under various flood scenarios, Engineering Structures 260 (2022) 114244.
[20] C. Friedl, et al., Assessing granular debris-flow impact forces on bridge superstructures, Journal of Bridge Engineering 29 (6) (2024) 04024027.
[21] E. Qiu, et al., Dynamic response characteristics of bridges under the impact of debris flows in mountainous areas, Physics of Fluids 37 (2) (2025).
[22] S.M.I. Kabir, H. Ahmari, M. Dean, Experimental study to investigate the effects of bridge geometry and flow condition on hydrodynamic forces, Journal of Fluids and Structures 113 (2022) 103688.
[23] S.M.I. Kabir, H. Ahmari, M. Dean, Contribution of debris and substructures to hydrodynamic forces on bridges, Engineering Structures 283 (2023) 115878.
[24] A. Hasanpour, D. Istrati, I.G. Buckle, Three-dimensional numerical investigation of floating debris effects on bridge superstructures during tsunamis, Ocean Engineering 289 (2023) 116262.
[25] W. Fan, et al., Reinforced concrete bridge structures under barge impacts: FE modeling, dynamic behaviors, and UHPFRC-based strengthening, Ocean Engineering 216 (2020) 108116.
[26] Z.H. Jin, et al., Simulations of debris flow impacting on bridge pier based on coupled CFD-DEM method, Ocean Engineering 279 (2023) 114532.
[27] X. Nan, et al., Study of the bridge damage during flooding based on a coupled VOF-FSI method, Journal of Engineering Research 11 (3) (2023) 51–61.
[28] Wang, Z., Y. Sha, and J.B. Jakobsen, *Floating bridge response under combined ship collision, wind and wave loads*. Ships and Offshore Structures: p. 1-18.
[29] H.Y. Luo, et al., Physics of building vulnerability to debris flows, floods and earth flows, Engineering Geology 271 (2020) 105611.
[30] F. Kalendher, et al., Analysis of flood impact on reinforced concrete (Pre-stressed) girder bridges–a case study, in: Proceedings of the 8th international Conference on Bridge Maintenance, Safety and Management (IABMAS 2016), University of Southern Queensland, 2016.
[31] H.A. Algaifi, et al., Optimizing polypropylene fiber and carbon nanotubes to reinforce concrete matrix: A response surface methodology, Construction and Building Materials 442 (2024) 137388.
[32] I. Abdulkadir, et al., Modelling and multi-objective optimization of the fresh and mechanical properties of self-compacting high volume fly ash ECC (HVFA-ECC) using response surface methodology (RSM), Case Studies in Construction Materials 14 (2021) e00525.
[33] D. Istrati, A. Hasanpour, I.G. Buckle, Numerical Investigation of Tsunami-Borne Debris Damming Loads on a Coastal Bridge, in: 17th World Conference on Earthquake Engineering, Sendai, Japan, 2020. Retrieved from, https://www.researchgate.net/publication/342027873.